Faraday Discuss., 2014, **171**, 93; DOI: 10.1039/c4fd00051j

Analysis of a Measurement Scheme for Ultrafast Hole Dynamics by Few Femtosecond Resolution X-ray Pump-Probe Auger Spectroscopy

Bridgette Cooper[a] , Přemysl Kolorenč[b], Leszek J. Frasinski[a], Vitali Averbukh[a] and Jon P. Marangos*[a]

Received Xth XXXXXXXXXX 20XX, Accepted Xth XXXXXXXXX 20XX
First published on the web Xth XXXXXXXXXX 200X
DOI: 10.1039/c000000x

Ultrafast hole dynamics created in molecular systems as a result of sudden ionisation are the focus of much attention in the field of attosecond science. Using the molecule glycine we show through *ab-initio* simulations that the dynamics of a hole, arising from ionisation in the inner valence region, evolve with a timescale appropriate to be measured using X-ray pulses from the current generation of SASE free electron lasers. The examined pump-probe scheme uses X-rays with photon energy below the K edge of carbon (275–280 eV) that will ionise from the inner valence region. A second probe X-ray at the same energy can excite an electron from the core to fill the vacancy in the inner-valence region. The dynamics of the inner valence hole can be tracked by measuring the Auger electrons produced by the subsequent refilling of the core hole as a function of pump-probe delay. We consider the feasibility of the experiment and include a numerical simulation to support this analysis. We discuss the potential for all X-ray pump-X-ray probe Auger spectroscopy measurements for tracking hole migration.

1 Introduction

Ultrafast hole migration, following sudden ionisation or excitation, is believed to be a universal response of extended molecules and is likely also to occur in some form in many condensed phase systems[1,2]. This process occurs due to the electron correlations within many-electron systems, and is predicted to take place typically on the few to sub-femtosecond timescale (i.e. into the attosecond time domain). It is currently a prominent goal in attosecond science to observe and fully characterise processes such as hole migration in order to: (a) deepen our understanding of the process and ascertain the role of hole migration in determining photochemical and photophysical outcomes, (b) to prove attosec-

[a] *Imperial College, Blackett Laboratory, Prince Consort Road, London, SW7 2BB, UK.; E-mail: b.cooper@imperial.ac.uk*
[b] *Institute of Theoretical Physics, Faculty of Mathematics and Physics, Charles University in Prague, V Holešovičkách 2, 18000 Prague, Czech Republic.*

ond measurement methods can address correlation driven dynamics in extended quantum systems such as biomolecules and polymers.

If we suddenly create a superposition of inner valence hole states in the cation of a moderately sized molecule (e.g. by photoionisation) we expect to see rapid evolution of this hole within the molecular frame. The most interesting class of dynamics occurs following the sudden formation of a hole state that is intrinsically a superposition of several eigenstates of the cation and so is expected to display non-exponential decay and time-dependent localisation. This may be due to the coupling of several one-hole (1h) electronic configurations or due to a coupling of a 1h configuration to a series of two-hole one-particle (2h1p) configurations of the cation by electron correlation. The superposition leads to a hole amplitude whose projection onto a single eigenstate may be seen to undergo rapid evolution. This may take the form of hole migration (i.e. motion of the hole around the molecular frame) or hole decay typically with some non-exponential (oscillatory) behaviour[3]. This will take place on a timescale that is short (< 10 fs) with respect to the timescale of nuclear motion[4]. We expect that the initial stages of the cation evolution to be dominated by electronic only motion (hole migration), with coupling to nuclear modes will become important at later times (charge transfer).

Both hole migration and non-exponential decay therefore stem from electron correlation and are currently of great interest to understanding ultrafast molecular science. Quantifying the role of electron correlation in multi-electron systems in a time-dependent way is a frontier challenge in ultrafast measurement. Moreover the problem of ultrafast hole evolution and motion is of critical importance to many aspects of photochemistry and photophysics where there is hitherto no experimental data at these short timescales[5,6]. An essential task is to find ways to measure time dependent information on the hole evolution and localisation in such situations. This task has up to now been prevented by the extremely fast timescales (few- to sub-femtosecond) of the hole motion. In what follows we will consider a scheme to use an X-ray pump–X-ray probe pulse sequence. The first pulse creates an inner valence hole (IVH) superposition that may undergo non-exponential decay. The second pulse then probes transitions from an inner shell to the hole state formed by the first pulse to give temporal information on the hole survival.

The current methods of attosecond science rely heavily on the process of high harmonic generation (HHG) as a means to generate attosecond pulses in the soft-X-ray photon energy range[7,8], but despite progress in the generation efficiency and shortness of the pulse duration[9,10] the power levels are currently found to be very low. This has prohibited the widespread application of attosecond pump-probe methods using the soft-X-ray pulses generated by HHG and instead techniques that replace one of the pulses with an infra-red high intensity field, either as the pump[11] or probe[12], have been commonly adopted. For example, the tracking of the dynamics of suddenly excited holes has recently been achieved in Kr atoms where the dynamics initiated by the strong field ionisation of a pair of spin-orbit split valence states was probed by transient absorption from an inner shell states[11]. In a similar scheme the dynamics of strong field ionisation in a SiO_2 solid state sample was tracked by measuring the holes created in the valence shell through transient absorption probing again from an inner shell

state[13]. Triggering ionisation through a strong field can lead, however, to significant complications since; (i) tunnel ionisation primarily accesses only the outer valence hole states, (ii) the tunnel ionisation process in a strong field is not fully understood and our theory for this in larger molecules remains to be adequately developed, (iii) the presence of a strong field may profoundly disturb the electron motion[14] in a molecule and so mask the underlying correlation driven effects.

In the light of the complications caused by strong-field ionisation it therefore seems necessary to resort to using the better understood process of single photon ionisation in a high frequency field if we are to trigger hole dynamics that are to be subject only to the intrinsic processes of a molecule. Pump-probe techniques based on measuring emission of IR or UV radiation emitted after sudden ionisation[15], using an XUV probe pulse and detection of HHG radiation[16] or measuring a double ionisation count via a single-photon laser enabled Auger decay (sp-LEAD)[17] scheme, have been proposed to measure correlation driven electron dynamics that occur in the inner-valence region in molecules. Although single photon ionisation is simple in principle, in practice we know from the discussion above that there is limited intensity from current attosecond pulses based upon HHG. This low intensity means we can in general hope to excite only a minuscule fraction of the sample during the short (few hundred attosecond pulse) thus making pump-probe experiments very challenging. Much effort is currently being put into generating HHG based attosecond sources with higher power[18]. This includes efforts to work with attosecond pulses[19,20] carried at lower frequency i.e. around 20 eV (rather than the conventional 90 eV), where the HHG processes is more efficient, and where the photoionisation cross-section in most molecules also tends to be relatively high. Hopefully these developments will permit the use of HHG based attosecond sources in the near future, but it is prudent to examine the potential for using alternative light sources to ensure that we can make progress on this problem.

X-ray free electron lasers (FELs) operating in SASE (self amplified spontaneous emission) mode are making rapid progress towards shorter pulse duration, and although not yet operating in the attosecond regime there are proposals that suggest this will be possible in the future[21]. Moreover X-ray FELs have already been demonstrated to generate pulses as short as a few femtoseconds when operating in the low bunch charge regime[22] or with a slotted emittance spoiler[23]. Given the very much higher pulse power of an X-ray FEL compared to a HHG source (we can expect single pulse photon numbers of $> 10^{11}$ for the former and typically $< 10^6$ for the latter) it is possible to contemplate efficient pump-probe excitation schemes in a FEL. This coupled to schemes that generate two-pulses, such as X-ray split-and-delay or a double slotted foil emittance spoiler, make possible high temporal resolution pump-probe measurements.

A problem in addition to the power requirements of pump pulse sources is that transient absorption, an attractive probe for attosecond measurements, requires not only a significant excitation fraction induced by the pump, but also a sufficiently dense sample to ensure measurable absorption. This may be readily achieved for condensed phase samples and for many molecular gases if suitable sample delivery is used. The prospects for biomolecules are typically more challenging since these have very low vapour pressures at temperatures that avoid thermally induced dissociation and this prohibits absorption studies. This means

we must seek alternative detection methodologies and we identify that Auger spectroscopy is a suitable state specific choice.

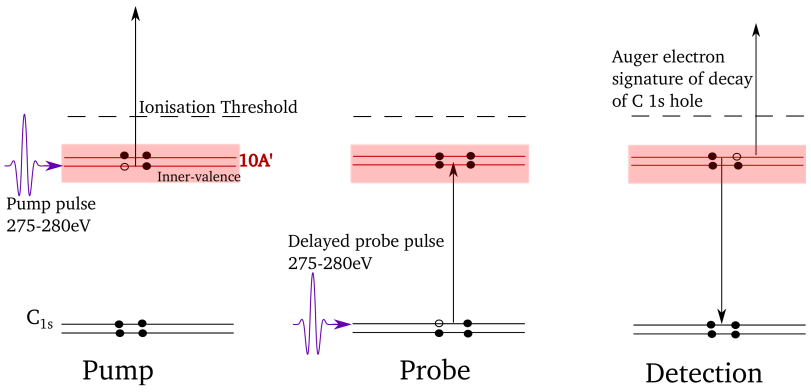

Fig. 1 Pump step opens a number of valence ionisation channels including creation of IVHs. The delayed probe pulse can strongly interact via a C 1s IVH transition (a channel only open if inner valence ionisation has occurred). Following this there can be Auger decay back to the C 1s hole with the emission of Auger electrons of characteristic energy that can be detected.

We discuss here a generic approach that would use an X-ray free electron laser to overcome the problems highlighted above. To demonstrate the feasibility of measurements of correlation driven dynamics in an amino acid we choose to analyse a concrete example accessible to currently operating X-ray FELs. The example we analyse is of non-exponential hole decay in glycine (rather than charge migration) which serves to demonstrate the feasibility of the scheme, but it would be applicable to a wider class of problem. The general concept, shown in Fig. 1 is that an X-ray FEL pulse is split into two with a small variable delay. Due to the high intensity of the FEL the first pulse can create a sufficient number of inner valence holes to be measured. The X-ray photon energy is, however, kept below the threshold for inner shell ionisation. The probe pulse, which may for convenience be at the same frequency, is tuned to resonance between an inner shell state in a carbon atom of the molecule and an inner valence state. If the inner valence state is filled no transition can occur, but if a hole has been formed by the first pulse then excitation may occur leaving a hole in the inner shell of the carbon atom. The strength of the transition is a probe of the probability of the hole and so can track the hole survival probability. Assuming the sample density is too low to apply absorption techniques we need to find an alternative way of measuring the probability of the inner valence hole. This can be done by registering the appearance of the core hole which will be refilled dominantly (for light elements) by Auger decay that results in a characteristic energy spectrum of emitted electrons. This is the detection scheme adopted in the example discussed below.

In the remainder of this paper we outline the details of the specific scheme and assess the experimental feasibility (Section 2), and then present a theoretical analysis of the hole dynamics in the inner valence states of glycine and our calculations of the effect of the coupling of the strong resonant X-ray fields on

the population dynamics in the cation (Section 3). We then discuss more general aspects of using X-ray laser pump-probe Auger spectroscopy for measuring hole migration before concluding (Section 5).

2 X-ray Laser Pump-Probe Auger Spectroscopy Scheme in Glycine

2.1 Scheme overview

Here we choose a simple molecule, the amino acid glycine (NH_2CH_2COOH) as an example for study. The three most abundant conformers of glycine are commonly referred to as Gly I, Gly II and Gly III[24,25] of which Gly I has the lowest energy. In a temperature range to have a sufficient amount of glycine in the gas phase $\sim 150-170\,^{\circ}C$, we expect the Gly I and Gly III conformers to dominate the sample at a ratio of approximately $2:1$[24]. We begin by calculating the ionisation spectra of the glycine conformers of interest, the results for the Gly I conformer are shown in Fig. 2. For this calculation and all subsequent calculations the inclusion of electron correlation into the wavefunctions to describe both the singly ionised and doubly ionised states is extremely important as electron correlation is driving the dynamics. Consequently where dipole moments, dynamics and Auger spectra are calculated, we use the Greens function technique called algebraic diagrammatic construction (ADC) to second order extended ADC(2)x[26], further details of which can be found in Section 3.

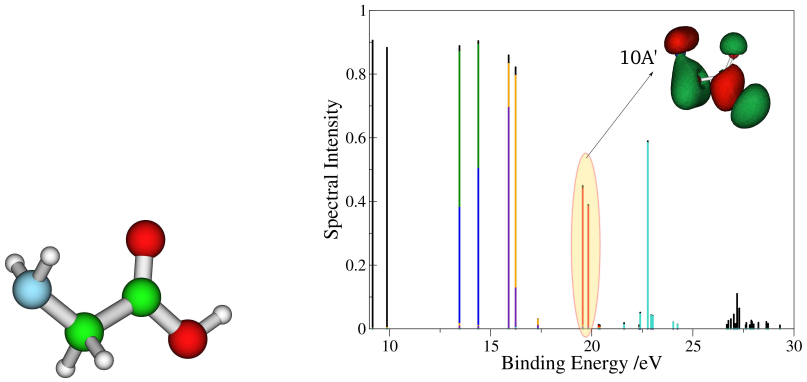

Fig. 2 Left: Glycine molecule NH_2CH_2COOH (blue N, red O, green C) geometry in the Gly I conformer. Right: Calculated energy spectrum of glycine with the states corresponding to ionisation from the 10A′ orbital highlighted. Insert shows the 10A′ orbital of glycine. Calculation performed using ADC(2)x with cc-pVDZ basis set augmented with 3s3p diffuse functions[27].

We concentrate on the inner valence hole associated with the 10A' state at around 20 eV binding energy (i.e. accessed by photon energies $\sim$275 eV), although there are other inner valence hole states that we expect to show interesting dynamics in this molecule. There are two eigenstates shown in the right panel of Fig. 2 (corresponding to the 10A′ molecular orbital), let us call them $|a\rangle$ and $|b\rangle$, which are each roughly 50% of a single 1h and 50% of a series of 2h1p

configurations. In this case the appearance of this doublet ($|a\rangle$ and $|b\rangle$) of mixed 1h-2h1p states and the resulting dynamics is caused purely by electron correlation. Only the 1h state can be created directly by sudden photoionisation so that at $t = 0$ we populate the hole which means we have a superposition of $|a\rangle$ and $|b\rangle$, say with "+" relative phase. As time goes by, the difference in the energies of the two states turns "+" into "−" and constructive interference that created a pure hole at $t = 0$ turns into destructive that brings the hole contribution to the wavepacket almost to zero. At this destructive interference time the wavepacket is almost purely composed of many different 2h1p's. Later on we go back to "+" and the hole experiences a revival. And so on until nuclear dynamics finally leads to a significant distortion of the molecular geometry (say, after 20 fs) changing the energies of the involved electronic states and so modifying or even damping the oscillations. This situation of evolution distinguishable over many femtoseconds is rather special to glycine because we only very rarely see breaking of a hole into two states with roughly equal hole contributions to them. Although in principle the same class of dynamics may occur in many other molecules, e.g. trans-butadiene for which we also have detailed calculations, there is not usually breaking of 1h into two states, but rather breaking into tens of states each of which is 90% or more 2h1p (so-called breakdown of molecular orbital picture of ionisation[28]), so to expect a full revival out of such complicated wavepacket is difficult. Nevertheless in these more typical systems it would be possible to follow the dynamics if higher (few hundred attosecond) temporal resolution were available.

Our calculations of the hole survival in the 10A' state, again using ADC(2)x are shown in Fig. 2 (see Section 3 for a more detailed discussion) for both the Gly I and Gly III conformers and for the the sum of Gly I and Gly III in a ratio of 2:1 expected from the operational temperature range. We see that the dynamics are sufficiently slow so that they are accessible to measurement using the temporal resolution available from e.g. the LCLS X-ray FEL located at SLAC. Whilst Fig. 3(a) and (b) shows that the dynamics for the Gly I and Gly III conformers show qualitatively similar oscillations there are differences in the periodicity and strength of the revivals, we expect that the signal measured will be dominated by the Gly I conformal evolution as is seen in Fig. 3(c). We will show that in glycine a hole created in the $10A'$ inner valence molecular orbital shows an oscillatory evolution on the timescale of $\sim$15 fs in our theoretical calculations (see Fig. 2 and Fig. 3). This dynamics would be easy to resolve with the temporal resolution available from LCLS. We illustrate the robustness of the measurement by simulating the effect of using an X-ray pulse of different durations, 2fs, 4 fs and 6 fs duration whereas we expect the pulse duration to be nearer 3 fs.

In the putative measurements an X-ray pulse from an X-ray FEL is split into a pair of identical X-ray pulses with a precisely controlled variable interpulse delay. Each of the pulses has a duration of only a few femtosecond. The photon energy of the pulses needs to be tuned to near 20 eV below the K edge of carbon in the molecule (requiring photons of around 275 eV from the FEL). The tuning is such that the X-rays cannot cause core shell ionisation or excitation in the molecule and so only valence shell ionisation can occur in the neutral molecule. If the photon energy is tuned to an appropriate value (say $\sim$275 eV) then following valence ionisation of the $10A'$ state a K shell (1s) to this inner valence

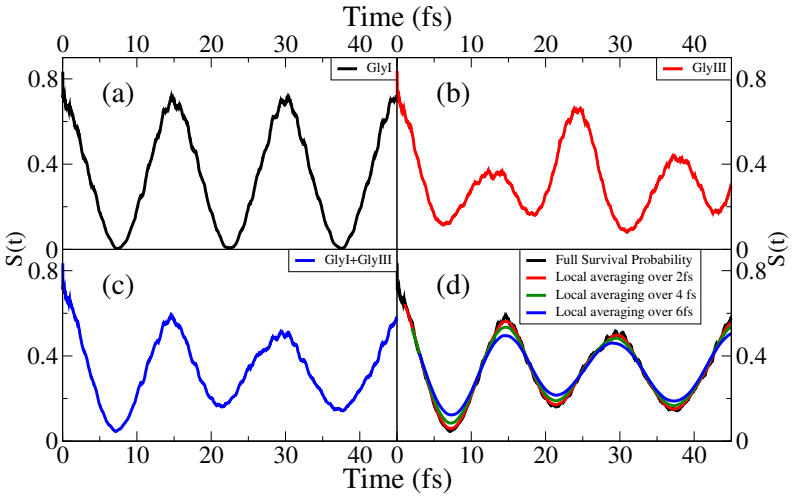

Fig. 3 Glycine 10A′ hole survival probability for (a) the Gly I conformer (black), (b) the Gly III (red), (c) the sum of Gly I and Gly III in a ratio of 2:1 expected from the operational temperature range (blue) and (d) the sum of Gly I and Gly III in a ratio of 2:1 (black) and normalised signal expected from a probe of the state population with a 2, 4 and 6 fs temporal resolution (red, green, blue). At times longer than 20 fs the signal is expected to be modified significantly by nuclear motion. Calculation of the survival probability was performed using ADC(2)x with cc-pVDZ basis set augmented with 3s3p diffuse functions[27].

hole (IVH) transition is opened up for the absorption of a second photon. This 1s IVH transition is allowed in the molecular system. We have calculated the dipole moment for the C K shell to IVH transition within the theoretical framework of this work and find a value of 2.8×10^{-31} Cm which is large enough to permit significant excitation probabilities for the X-ray laser intensities likely to be used (see next section).

The extra absorption registers the existence of the inner valence hole and if that hole is evolving in time the excitation probability as a function of pump-probe delay will reflect this. The Auger electron signal associated with the subsequent refilling of the 1s core hole is characteristic of the channel and so we can to use this signature to track the hole dynamics (see Fig. 1). We calculate the spectrum of Auger electrons that will be emitted from the glycine cation when the inner shell hole is refilled using Fano-ADC(2)x method for the partial decay widths[29], and ADC(2)x method for singly and doubly[30] ionised energies in aug-pCVQZ basis without g functions, uncontracted on the C centres. The calculated spectrum is shown in figure 4.

2.2 Experimental implementation: Feasibility with current X-ray FEL sources

It is our conjecture that already SASE X-ray FEL light sources offer parameters required to implement this measurement scheme. As a concrete example we choose to consider the LCLS facility at Stanford. There are several alternative operating modes of an X-ray FEL, such as LCLS, that can provide the required

X-ray pump–X-ray probe pulses. The simplest method is to use a single short pulse (created in the low bunch charge mode or with a single slotted foil) and then to employ an X-ray split-and-delay apparatus. The requirement on photon energy (275 eV) and the short pulses ($\sim$3 fs) will mean the pulse peak power will be relatively low compared to that potentially available with an X-ray FEL. We estimate around $100\mu J$ can be generated at this pulse energy and accounting for transfer optics $\sim$10 μJ will reach the target in a spot size of $\sim$10 μm to achieve an intensity $\sim 10^{15}$ Wcm^{-2}. In fact the relatively low intensity, compared to the much higher intensities often used in X-ray FEL experiments, is advantageous in this case as it is important to operate in the linear interaction regime for each pulse and to avoid opening additional excitation and ionisation channels in the molecule that might lead to increased background.

The sample can be introduced as a gas to the X-ray interaction region via an effusive beam from a nozzle. This requires the sample to be heated in an oven (operating in the temperature range $\sim$150–210 °C) in proximity to the interaction region[31] as has been used successfully in a number of synchrotron based experiments where sufficient densities for NEXAFS and photoelectron experiments in glycine were demonstrated. It is from this earlier work that we obtain the carbon K edge values in this molecule. It is required to work in the lower part of the available temperature range of the oven ($150-170\,^{\circ}$C) to ensure the sample population is dominated by the Gly I and III conformers which our calculations show sufficiently similar dynamics for the IVH states of interest (see Fig. 3). With an oven operating at these temperatures we would expect to achieve densities[32,33] 10^{13}–10^{15} cm^{-3} which will translate into densities up to $\sim 10^{12}$ cm^{-3} in the interaction region. The use of methods for conformer separation[34] could be used to enable the study of the dynamics of a single conformer.

There will be no core electron ionisation in the glycine molecule from a single photon at an energy of 275 eV. The valence photoionisation (VP) will open up a lot of channels that form the background. However the photoelectron energies from these valence electrons will sit a few tens of eV away from the Auger transitions of interest. In the IPI-CE-AU process (inner-valence photoionisation, core-excitation of 1s to IVH, Auger decay) we will have two correlated electrons: eIPI and eAU. The kinetic energies will be; eIPI $\sim$270–250 eV (for the photon energies planned) and eAU $\sim$260–230 eV. We therefore find much of the Auger spectrum (see calculated spectrum Fig. 4) at photon energies lying well outside of the valence photoelectron range. It should therefore be easy to identify the IPI-CE-AU process which is the signature of the IVH. The Auger photoelectron spectrum must be recorded with sufficient energy discrimination; an electron magnetic bottle TOF spectrometer is a suitable instrument for this in that it provides high energy energy resolution ($\sim$1 eV) and a high collection efficiency that ameliorates the low sample density. The electron energy spectrum will therefore isolate the nearby photoelectrons from the characteristic Auger electrons that arise from the decay of the C K-shell hole.

Additionally one can use covariance mapping to further increase the visibility of the signal. An "island" in the covariance map corresponding to these kinetic energies should be present. It has previously been demonstrated that electron-electron covariance is feasible at FELs (at both FLASH and LCLS)[35,36]. Other processes that will give two correlated electrons in the same energy range are

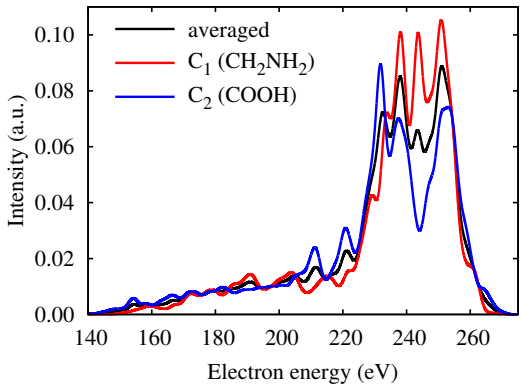

Fig. 4 The calculated Auger spectra for the C1s vacancies in glycine, calculated using Fano-ADC(2)x method for the partial decay widths, and ADC(2)x method for singly and doubly ionised energies in aug-pCVQZ basis without g functions, uncontracted on the C centres.

two sequential photoionisations (IPI-VP, IPI-IPI, VP-IPI, VP-VP) from valence or inner valence. We can measure these separately by examining shots where the pulse is detuned from resonance, so that it does not induce the core excitation, and so account for their contribution. Moreover the cross section will be lower (at least compared to a IPI-CE-AU process).

The sample density available is sufficiently high (we estimate that there will be up to 10^5 molecules within the 10^{-7}cm^3 interaction region) that the acquisition limit will be set by space charge effects rather than available sample density. The focal spot is 10 μm diameter and the X-rays per 10 μJ pulse will give a total valence ionisation probability of 0.16 so giving $\sim 1.6 \times 10^4$ electrons per shot at the higher sample density. Taking a conservative number of 1000 electrons/shot (based upon previous experience with the magnetic bottle instrument) to avoid space charge effects we can proceed with the estimate. Using empirical data the probability of L shell holes (IVH) being created in each ionised molecule is 0.125. Next we estimate the probability of excitation 1s IVH in the second pulse using our calculated dipole moment. Assuming the laser intensity to be $10^{15} W cm^{-2}$ we can expect the excitation from the inner shell to be at least 0.1 and a probability of the subsequent Auger electrons falling into the suitable energy band can be estimated to be > 0.25 (see calculated spectrum Fig. 4).

Next we must consider the intrinsic fluctuations of a SASE FEL generated X-ray pulse. Because we employ an X-ray pump- X-ray probe scheme the delay is immune to the absolute timing jitter of the X-ray pulse. Moreover in the low bunch charge operation the emission is expected to be overwhelmingly in a single X-ray pulse, rather than the more complex X-ray pulse temporal structures commonly encountered when using SASE with a high bunch charge. Nevertheless we can expect significant shot-to-shot spectral fluctuations of the SASE spectrum. Whilst the bandwidth of an individual pulse will be in the region of 1 eV the SASE fluctuation can lead to a spectrum (averaged over fluctuations) around 10 times broader. Fortunately the photon energy spectrum for each shot can be measured via a number of channels, e.g. using an X-ray spectrometer or the elec-

tron bunch energy diagnostic. Thus the resonant shots can be selected from the data set and the non-resonant shots used to characterise the VP background.

Collecting the numbers above the total number of counts per shot will be $1000 \times 0.125 \times 0.1 \times 0.25 \approx 3$ or 360 per second. Assuming in photon energy binning the effective shot rate is reduced by an order of magnitude, at the operational repetition rate of LCLS of 120 Hz we have in 20 minutes a count of 4.3×10^4 electrons in the energy region of interest (i.e. a count rate shot noise error of below 0.5%), which indicates the feasibility of measuring the required signals using existing light sources. A detailed analysis of the experimental s/n of course must await the actual execution of an experiment.

3 Theoretical modelling of X-ray the pump-probe measurements of hole survival probability in glycine

Here we model the effects of the strong resonant X-ray probe pulse on the Auger electron yield. The purpose of this is to model the anticipated experimental signals and to confirm that under the likely conditions of a real experiment where the pulse intensities are high enough to give measurable signals the x-ray pump pulse will not significantly perturb the inner valence state dynamics it has excited. We do this by following the methodology set in the work of Rohringer and Santra[37] generalised for the case of two initial states that is relevant to the hole migration dynamics that occurs in glycine. Throughout we will assume the Gly I conformer of glycine, as Fig. 3 shows that in the anticipated experimental conditions the dynamics of this conformer dominates.

At $t = 0$ we assume that the first 275 eV pulse (the pump) has created a superposition of two cationic states $|a\rangle$ and $|b\rangle$ corresponding to ionisation from the 10A′ molecular orbital in glycine:

$$\Psi^{(N-1)}(t=0)\rangle = \tilde{c}_a(t=0)|a\rangle + \tilde{c}_b(t=0)|b\rangle. \tag{1}$$

Ionising from the 10A′ orbital produces states that are below the double ionisation threshold, and therefore are Auger inactive. However, each state has a large contribution of 2h1p configurations as the calculated spectral intensity spectrum for glycine shows in Fig. 2. The temporal evolution of the superposition of the states created when ionising from the 10A′ orbital can be fully characterised by the survival probability of the initial state, $S(t)$:

$$S(t) = \left||\tilde{c}_a|^2 \exp(-iE_a t) + |\tilde{c}_b|^2 \exp(-iE_b t)\right|^2, \tag{2}$$

where E_a and E_b are the energies of the cationic eigenstates $|a\rangle$ and $|b\rangle$ respectively, (atomic units are used throughout). In the case of ionisation from the 10A′ the resulting dynamics (see Fig. 3) show an oscillatory evolution of the survival probability involving coupling of a 1h state to a manifold of bound ionic states of the 2h1p type.

At a delay time t after the initial ionisation event, a probe pulse, also of 275 eV, induces a transition from a carbon 1s orbital to fill the inner valence 10A′ orbital producing state $|1s\rangle$. In the case of glycine, there are two carbon 1s orbitals: 4A′ located on the carboxyl group and 5A′ the C centre attached to the amine group. In the following simulation of pump-probe experiment we assume

that the width of the probe pulse is insufficient to span both core orbitals, and sum incoherently. In the following, we assume that a core ionised state couples the initial superposition of states only via the dipole interaction $\varepsilon(t)\hat{z}$. This assumption excludes any single-photon laser-enabled Auger decay (sp-LEAD) transitions[17] from the initial superposition of states directly to the final states. Thus, if the field free Hamiltonian is denoted as $\hat{H}_0$ the Hamiltonian in the presence of the electric field is given by:

$$\hat{H}(t) = \hat{H}_0 + \varepsilon(t)\hat{z}. \tag{3}$$

The core ionised states will decay via Auger transitions into the final states $\sum_i \int \mathrm{d}\varepsilon_i \tilde{g}_i(\varepsilon_i,t)|i,\varepsilon_i\rangle$ where i is the ith eigenstate of the glycine cation and ε_i the resonant Auger electron associated with that channel. By using Wigner-Weisskopf theory[38], the partial decay width Γ_i associated with the irreversible transition from $|1\mathrm{s}\rangle$ to $|i,\varepsilon_i\rangle$ can be written as:

$$\begin{aligned} \Gamma_i &= 2\pi \left|\langle i,\varepsilon_i|\hat{V}_C|1\mathrm{s}\rangle\right|, \\ \Gamma_{1s} &= \sum_i \Gamma_i, \end{aligned} \tag{4}$$

where $\hat{V}_C$ is the Coulomb operator. In our numerical simulations, the partial widths will be taken from an Fano-ADC theory, where the widths are given by the matrix elements of the total Hamiltonian less the energy of the resonance[29]. The wavefunction to describe the cationic system as a function of time is thus:

$$\Psi^{(N-1)}(t)\rangle = \tilde{c}_a(t)|a\rangle + \tilde{c}_b(t)|b\rangle + \tilde{c}_{1\mathrm{s}}(t)|1\mathrm{s}\rangle + \sum_i \int \mathrm{d}\varepsilon_i \tilde{g}_i(\varepsilon_i,t)|i,\varepsilon_i\rangle. \tag{5}$$

We consider a symmetric probe pulse, with the detuning of the with respect to the resonant transitions is given by:

$$\delta = E_{1\mathrm{s}} - \frac{(E_a+E_b)}{2} - \omega, \tag{6}$$

where E_a and E_b are the eigenstate energies of the two states making up the superposition of the initial state, $E_{1\mathrm{s}}$ is the energy of the core ionised state, and the central frequency is given by $E_{1\mathrm{s}} - (E_a+E_b)/2$. Thus the amplitude of the field for the transition from the core 1s ionised state to the inner valence state $|a\rangle$ will be the same as for the transition to state $|b\rangle$. The field is assumed to be linearly polarised in the x direction with the field strength given by:

$$\varepsilon(t) = \varepsilon_c(t)\cos(\omega_x t) + \varepsilon_s(t)\sin(\omega_x t), \tag{7}$$

where $\varepsilon_c(t)$ and $\varepsilon_s(t)$ are assumed to be slowly varying compared to $2\pi/\omega_x$.

For the expansion coefficients appearing in the total wavefunction (Eq. 5 we make the following ansatz:

$$\begin{aligned} \tilde{c}_{\{a,b\}}(t) &= c_{\{a,b\}}(t)\exp\left[-i\left(E_{1\mathrm{s}} - \frac{E_{\{a,b\}}-E_{\{b,a\}}}{2} + \delta/2\right)t\right], \\ \tilde{c}_{1\mathrm{s}}(t) &= c_{1\mathrm{s}}(t)\exp\left[-i\left(E_{1\mathrm{s}} - \frac{E_a-E_b}{2} - \delta/2\right)t\right], \\ \tilde{g}_i(\varepsilon_i,t) &= g_i(\varepsilon_i,t)\exp\left[-i\left(E_{1\mathrm{s}} - \frac{E_a-E_b}{2} - \delta/2\right)t\right]. \end{aligned} \tag{8}$$

Equations of motion for the initial states in the superposition can be found by substituting Eq. 5 into Eq. 3 using the expansion coefficients given in Eq. 8 and applying the rotating wave approximation to give:

$$i\dot{c}_a(t) = -\frac{\delta}{2}c_a(t) + \frac{\mathcal{R}_a^*(t)}{2}c_{1\mathrm{s}}(t)\exp\left(-i\frac{E_b - E_a}{2}t\right), \quad (9)$$

$$i\dot{c}_b(t) = -\frac{\delta}{2}c_b(t) + \frac{\mathcal{R}_b^*(t)}{2}c_{1\mathrm{s}}(t)\exp\left(-i\frac{E_a - E_b}{2}t\right), \quad (10)$$

where the Rabi frequency $\mathcal{R}_a(t)$ is given by:

$$\mathcal{R}_a(t) = \langle 1\mathrm{s}|\hat{z}|a\rangle\{\varepsilon_c(t) + i\varepsilon_s(t)\}. \quad (11)$$

To obtain the equation of motion for the resonant core-ionised state, we treat the decay of this state into the manifold of Auger final states in the standard manner[37,38]:

$$i\dot{c}_{1\mathrm{s}}(t) = \frac{\delta}{2}c_{1\mathrm{s}}(t) + \frac{\mathcal{R}_a(t)}{2}c_a\exp\left(-i\frac{E_a - E_b}{2}t\right) + \frac{\mathcal{R}_b(t)}{2}c_b\exp\left(-i\frac{E_b - E_a}{2}t\right) - ic_{1\mathrm{s}}(t)\frac{\Gamma_{1\mathrm{s}}}{2}, \quad (12)$$

with the total decay width $\Gamma_{1\mathrm{s}}$ given by Eq. 4. The equation of motion for the final Auger states are expressed as

$$i\dot{g}_i(\varepsilon_i,t) = \left(E_i^{2+} + \varepsilon_i - E_2 + \frac{\delta}{2}\right)g_i(\varepsilon_i,t) + c_{1\mathrm{s}}(t)\sqrt{\frac{\Gamma_i}{2\pi}}, \quad (13)$$

with E_i^{2+} the energy of the doubly ionised state and ε_i the energy of the Auger electron in the continuum.

Finally the resonant Auger electron line profile associated with the *i*th decay channel is given as[37]

$$P_i(\varepsilon_i) = \lim_{t\to\infty}|g_i(\varepsilon_i,t)|^2. \quad (14)$$

Within this model, the area under the resonant Auger electron line profile will evolve with a frequency related to the energy difference between the two states, $|a\rangle$ and $|b\rangle$ that constitute the initial superposition, as can be seen from Eqs. 12, 13.

3.1 Numerical results

The dynamics of the inner valence hole are driven by electron correlation and therefore the multi-electron states must include configuration interaction. We describe the inner valence ionised initial state, the core ionised decaying (Auger-active) state and the doubly ionised final states using the ADC(2)x *ab initio* method, which represents the $(N-1)$-electron wavefunction in a basis of intermediate states of 1h (ϕ_i) and 2h1p (ϕ_{ij}^a) classes derived from the perturbation theoretically corrected HF ground state of the neutral[26].

$$\Psi^{(N-1)} = \sum_i c_i\phi_i + \sum_{ija} c_{ij}^a\phi_{ij}^a, \quad (15)$$

where i, j are hole indices (occupied HF orbitals of the neutral) and a is a particle index (unoccupied HF orbital of the neutral). ADC(2)x describes the 1h-like initial and core-ionised states up to second order in the many-body perturbation theory, while the 2h1p-like final Auger states are described up to first order. The energies of the final states and the partial widths are calculated using Fano-ADC theory, where the widths are given by the matrix elements of the total Hamiltonian minus the energy of the resonance[29] and Stieltjes imaging to energy renormalise the final state wavefunction. The basis sets used are Gaussian $\mathcal{L}^2$ bases supplemented with extra diffuse functions[27] to better describe the continuum states. This methodology is used in all the calculations presented in this discussion.

For our numerical simulations we have assumed a Gaussian temporal envelope for ε_c and set $\varepsilon_s = 0$. The amplitude of the field is 5.14×10^{11} Vm^{-1} with a the root-mean-squared (RMS) width of 2 fs and zero detuning, $\delta = 0$. We assume a uniform intensity distribution; thus spatial averaging over the pulse is not performed. The equations of motion (Eqs. 9-13) discussed in the previous section are solved using a standard fourth order Runge-Kutta integrator.

In contrast to the survival probability shown in Fig 3, we first calculate the survival probability of the initial superposition of states when the electric field is applied. This is calculated assuming an equal population of the the state $|a\rangle$ as the state $|b\rangle$, that is $\tilde{c}_a(t=0) = \tilde{c}_b(t=0) = 1/\sqrt{2}$, and inserting the wavefunction at $t' = 0$ (Eq. 1) and the wavefunction at a time t' (Eq. 5), where t' is the propagation time, into the survival probability:

$$\begin{aligned} S(t') &= \left|\langle\Psi^*(t'=0)|\Psi(t')\rangle\right|^2 \\ &= \left|\tilde{c}_a^*(t'=0)\tilde{c}_a(t') + \tilde{c}_b^*(t'=0)\tilde{c}_b(t')\right|^2. \end{aligned} \tag{16}$$

Using the above parameters for the pulse, and choosing a probe delay time of 1.2 fs the survival probability of the initial superposition of states is shown in Fig. 5, where the probe pulse transfers the hole to the amino group in (a) and to the carboxyl group in (b). After the probe pulse has passed, population has been transferred to the core-ionised state shown in the reduction of the amplitude, but the remaining population in the initial states shows the same temporal evolution as that shown in Fig 3 consisting of oscillations with a period of about 15 fs. The underlying dynamics of the initial state have not been destroyed upon application of the the probe pulse, therefore it can be considered as perturbative, even in a field somewhat higher than that required in an experiment. In the equations of motion for the initial states in Eq. 9 the dipole coupling between the states, $|a\rangle$ and $|b\rangle$ has been neglected. However, our simulations show that inclusion of this direct high-frequency dipole coupling between these two closely lying states leads to sub-percent corrections with the pulse parameters chosen of 5.14×10^{11} Vm^{-1}. $|c_{2s}|^2$ gives a measure of the transfer of population to the core ionised state resulting from the application of the pulse. Fig. 5 also shows that there is more transfer of population to the core-ionised state where the hole is located on the carbon nearest the amino group. This is because the transition matrix elements are approximately 2.5 times larger for transfer from the amino group to the 10A' superposition of states compared to transitions from the carboxyl group. The core-ionised state decays to away to zero within 10 fs as a result of coupling to the final Auger states.

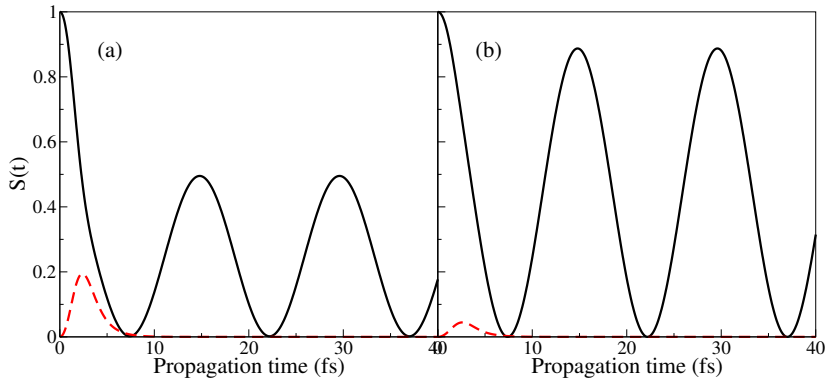

Fig. 5 Survival probability of the initial superposition of states (black), and the probability of populating the core-ionised state $|c_{1s}|^2$ (red dashed line), (a) core ionised from the CH_2NH_2 group and (b) core ionised from COOH. as a function of propagation time. The probe pulse is centred at 1.2 fs. with an root-mean-squared width of 2 fs.

The detection part of the pump-probe scheme detailed in Section 2 involves the measurement of the Auger yield as a function of pump-probe delay. We calculate this using Eq. 14 where we propagate the equations of motion (Eqs. 9-13) for 96 fs, considerably further than after the probe pulse has passed. Fig. 6 shows the variation of the Auger yield as a function of pump probe delay. As expected from the analysis of the equations of motion, the modulation in the Auger yield has a frequency related to the energy difference between the two initial states ($|a\rangle$ and $|b\rangle$) and demonstrates that this measurement of the Auger yield successfully captures the dynamics that are characterised by the survival probability shown in Fig. 3. In our present model, we assume that the probe pulse does not have the spectral breadth to couple the two possible core ionised channels. We therefore calculate the Auger yield from each channel separately and sum incoherently. From the survival probabilities Fig. 5 we expect the yield from the amino channel to dominate the expected Auger yield as a function of time because of the differences in the magnitudes of the transition matrix elements.

Finally we show that it is just the magnitude of the Auger profile that changes as a function of the pump-probe delay, as can be seen in Fig. 7. This shows the Auger profile as a function of the energy of the emitted electron for different pump-probe delays. The probe delays correspond to the maxima in Fig 6 at approximately 14.5 fs, an intermediate time of 10.3 fs, and finally immediately after the minima occurring at 7.3 fs. In each case, the shape of the Auger profile remains the same, and only the amplitude oscillates as a function of pump-probe delay.

4 Discussion

The preceding analysis examines the feasibility of the proposed scheme. The dynamics of conformers Gly I and Gly III are similar and the measured signal will be the result of the weighted sum from these two conformers (plus a small contribution from Gly II). With an expected ratio of 2:1 for Gly I and Gly III

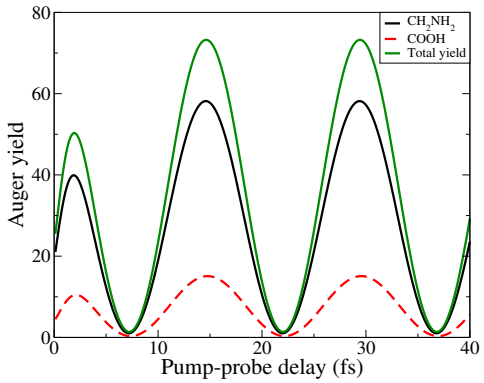

Fig. 6 Auger profile as a function of pump-probe delay. The Auger profile shows the same modulation of signal as is seen in the survival probability of the initial states, which is associated with the energy difference between the two states $|a\rangle$ and $|b\rangle$ that make up the superposition.

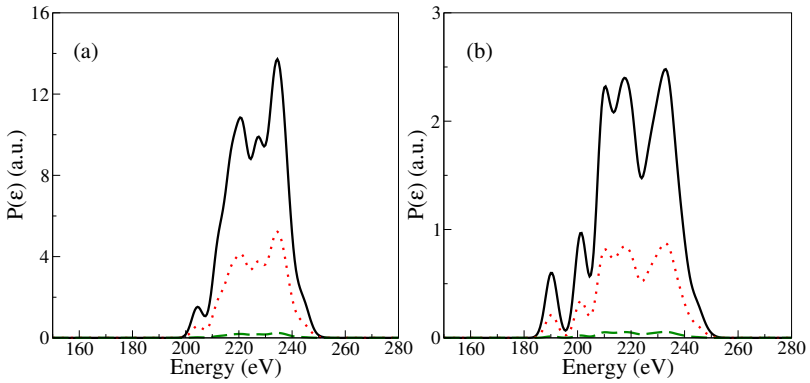

Fig. 7 Calculated Auger profile as a function of energy with vibrational broadening. (a) Spectrum associated with a core vacancy on the CH_2NH_2 and (b) with the vacancy on the COOH carbon centre. The Auger profile at three different pump-probe delays is shown: in black at 14.5 fs corresponding to the first maxima in Fig. 6, in red at 10.3 fs, and in green at 7.3 fs corresponding to just after the first minima in Fig. 6. The entire Auger spectrum is modulated as a function of pump-probe delay.

respectively, we anticipate the dynamics of Gly I to dominate the observed signal. As we noted earlier the concentration of the Gly II conformer is likely to be low for the temperatures likely to be used. Conformer selection is thought to be possible for glycine (J.Kupper, Private Communication) and this would permit signals from a pure sample of a single conformer to be measured.

Of course the simple behaviour that arises purely from the electron dynamics in the glycine will not persist indefinitely. The nuclear dynamics will be revealed by modifications of the oscillation period and amplitude of the hole survival probability that is measured. So far we have not included this into our calculations, but in principle this can be done and this will be required to extract both electronic and nuclear dynamics from the measured signal.

We now turn to the further prospect for X-ray pump - X-ray probe Auger spectroscopy. An extension to measuring faster time-scale dynamics is immediately possible if shorter X-ray pulses can be generated from X-ray FELS. Whilst it is not yet certain, it is likely, that by optimising the operation of a SASE FEL a pulse as short as 1 fs may be attainable. There are schemes under consideration that may in future generate pulses as short as 100 attosecond or even less. Thus it can be hoped that in the future a wide range of ultrafast molecular hole dynamics can be measured by X-ray pump-probe Auger spectroscopy.

Another promising direction is to follow hole migration in space as well as time via this technique. In the glycine example we do not expect a significant time dependence in the hole localisation, only in the overall survival probability. The chemical shift of the C K shell at the amine and carboxyl sites could, in principle, be used to register any differences in the hole survival at the two sites. It would allow the separate measurement of the hole survival probability localised at the amine and carboxyl sites of a molecule. The actual feasibility of this will depend upon the details of the X-ray pulse spectral bandwidth. If the pulse bandwidth is near 1 eV or less (i.e. much smaller than the C K edge shift between these two sites which is several electron volts) we can anticipate that the pulse will either interact with the amine or the carboxyl site depending upon the tuning of that individual pulse. The data for each channels evolution could thus be separately measured by sorting the data on the photon energy. Such an idea may be extended to measuring hole migration in larger biomolecules.

It is of course possible to use an atom different from the C, N or O common in a biomolecule as a spatial marker to localise the hole survival. Atoms such as S, P and Cl, which have K edges at 2470 eV, 2140 eV and 2820 eV respectively, might occur at only one or a few sites within a larger molecule. Resonant excitation into IVH states from the K shells of these atoms could be used to localise the hole evolution in space and time. These high energy photons will now also cause inner shell ionisation and excitation of C, N and O atoms in the same molecule. However, as the photon energy is significantly higher than the edges of the latter species the cross-sections for these processes will be relatively low. This fact, combined with the anticipated unique Auger spectrum of the inner shell decay of the spatial marker atom, may allow the method to be applied to a wide range of molecules.

5 Conclusion

We have shown that it is possible to measure correlation driven electron dynamics in an amino acid with the X-ray pump-probe technique combined with Auger electron detection. Whilst not all of the correlation driven hole migration processes that one would wish to study have dynamics slow enough to be accessible to the current X-ray FEL pulse duration (3 fs) there are some important classes that are accessible in certain molecules. These are the non-exponential evolutions of superpositions of charge states associated with frustrated Auger decay that occur when inner-valence states are suddenly ionised[39]. Glycine is a molecule that has proved in our theoretical calculations to be highly suitable to observe these somewhat slowed hole migration effects. What is proposed is that a first pulse creates (suddenly) a superposition of hole states in the glycine molecule. Given that the K edge for the two carbons in glycine are at 292.5 eV and 295 eV the X-ray energy needs to be near 270 eV since the binding energy of the states of interest are around 20 eV. The required pulse duration is $\sim$3 fs and the energy bandwidth for a single pulse $>$ 1 eV, with the second pulse nominally identical. The second pulse can then cause photoabsorption from the 1s state into the hole superposition created.

This work indicates that it is feasible to use an X-ray FEL to measure the ultrafast electronic dynamics driven by electron correlation within a typical molecular system (amino acid), a capability that would pave the way to applications to larger molecules (e.g. peptides) and condensed phase systems. In principle, the method can be extended to measuring hole migration in larger molecules as the specific atomic core state to inner valence hole transition probability provides time-dependent localisation information for the inner valence hole.

6 Acknowledgements

The authors acknowledge the financial support of the Engineering and Physical Sciences Research Council (EPSRC, United Kingdom) through the Programme Grant on Attosecond Dynamics (award EP/I032517/1) and the ERC ASTEX project 290467. V.A. acknowledges EPSRC through the Career Acceleration Fellowship (award EP/H003657/1). P.K. acknowledges the support from the Czech Science Foundation (Project GACR P208/12/0521).

References

1 (*a*) F. Remacle and R. D. Levine, *Proceedings of the National Academy of Science*, 2006, **103**, 6793; (*b*) A. I. Kuleff and A. Dreuw, *The Journal of Chemical Physics*, 2009, **130**, 034102; (*c*) H. Eshuis and T. van Voorhis, *Physical Chemistry Chemical Physics*, 2009, **11**, 10293.

2 J. Breidbach and L. S. Cederbaum, *The Journal of Chemical Physics*, 2003, **118**, 3983.

3 V. Averbukh, U. Saalmann and J. M. Rost, *Physical Review Letters*, 2010, **104**, 233002.

4 D. Mendive-Tapia, M. Vacher, M. J. Bearpark and M. A. Robb, *The Journal of Chemical Physics*, 2013, **139**, 044110.

5 L. S. Cederbaum and J. Zobeley, *Chemical Physics Letters*, 1999, **307**, 205.

6 R. Weinkauf, E. W. Schlag, T. J. Martinez and R. D. Levine, *The Journal of Physical Chemistry A*, 1997, **101**, 7702.

7 M. Drescher, M. Hentschel, R. Kienberger, G. Tempea, C. Spielmann, G. A. Reider, P. B. Corkum and F. Krausz, *Science*, 2001, **291**, 1923–1927.

8 F. Frank, C. Arrell, T. Witting, W. A. Okell, J. McKenna, J. S. Robinson, C. A. Haworth, D. Austin, H. Teng, I. A. Walmsley, J. P. Marangos and J. W. G. Tisch, *Review of Scientific Instruments*, 2012, **83**, 071101.

9 F. Ferrari, F. Calegari, M. Lucchini, C. Vozzi, S. Stagira, G. Sansone and M. Nisoli, *Nature Photonics*, 2010, **4**, 875–879.

10 T. Popmintchev, M.-C. Chen, P. Arpin, M. M. Murnane and H. C. Kapteyn, *Nature Photonics*, 2010, **4**, 822–832.

11 E. Goulielmakis, Z.-H. Loh, A. Wirth, R. Santra, N. Rohringer, V. S. Yakovlev, S. Zherebtsov, T. Pfeifer, A. M. Azzeer, M. F. Kling, S. F. Leone and F. Krausz, *Nature*, 2010, **466**, 739.

12 A. L. Cavalieri, N. Müller, T. Uphues, V. S. Yakovlev, B. Horvath, B. Schmidt, L. Blümel, R. Holzwarth, S. Hendel, M. Drescher, U. Kleineberg, P. M. Echenique, R. Kienberger, R. Krausz and U. Heinzmann, *Nature*, 2007, **449**, 1029.

13 M. Schultze, E. M. Bothschafter, A. Sommer, S. Holzner, W. Schweinberger, M. Fiess, M. Hofstetter, R. Kienberger, V. Apalkov, V. S. Yakovlev, M. I. Stockman and F. Krausz, *Nature*, 2013, **493**, 75.

14 M. Lezius, V. Blanchet, M. Y. Ivanov and A. Stolow, *The Journal of Chemical Physics*, 2002, **117**, 1575.

15 A. I. Kuleff and L. S. Cederbaum, *Physical Review Letters*, 2011, **106**, 053001.

16 J. Leeuwenburgh, B. Cooper, V. Averbukh, J. P. Marangos and M. Ivanov, *Physical Review Letters*, 2013, **111**, 123002.

17 B. Cooper and V. Averbukh, *Physical Review Letters*, 2013, **111**, 083004.

18 F. Lépine, G. Sansone and M. J. J. Vrakking, *Chemical Physics Letters*, 2013, **578**, 1–14.

19 J. Henkel, T. Witting, D. Fabris, M. Lein, P. L. Knight, J. W. G. Tisch and J. P. Marangos, *Physical Review A*, 2013, **87**, 043818.

20 D. Fabris, W. A. Okell, T. Witting, J. P. Marangos and J. W. G. Tisch, *pre-print*, arXiv:1311.4738.

21 A. A. Zholents and W. M. Fawley, *Physical Review Letters*, 2004, **92**, 224801.

22 Y. Ding, A. Brachmann, F.-J. Decker, D. Dowell, P. Emma, J. Frisch, S. Gilevich, G. Hays, P. Hering, Z. Huang, R. Iverson, H. Loos, A. Miahnahri, H.-D. Nuhn, D. Ratner, J. Turner, J. Welch, W. White and J. Wu, *Physical Review Letters*, 2009, **102**, 254801.

23 Y. Ding, F.-J. Decker, P. Emma, C. Feng, C. Field, J. Frisch, Z. Huang, J. Krzywinski, H. Loos, J. Welch, J. Wu and F. Zhou, *Physical Review Letters*, 2012, **109**, 254802.

24 J. J. Neville, Y. Zheng and C. E. Brion, *Journal of the American Chemical Society*, 1996, **118**, 10533.

25 A. G. Császár, *Journal of the American Chemical Society*, 1992, **114**, 9568.

26 A. B. Trofimov and J. Schirmer, *The Journal of Chemical Physics*, 2005, **123**, 144115.

27 K. Kaufmann, W. Baumeister and M. Jungen, *Journal of Physics B*, 1989, **22**, 2223.

28 J. S. L.S. Cederbaum, W. Domcke and W. von Niessen, *Adv. Chem. Phys.*, 1986, **65**, 115.

29 V. Averbukh and L. S. Cederbaum, *The Journal of Chemical Physics*, 2005, **123**, 204107.

30 J. Schirmer and A. Barth, *Zeitschrift für Physik A*, 1984, **317**, 267.

31 R. R. Blyth, R. Delaunay, M. Zitnik, J. Krempasky, R. Krempaska, J. Slezak, K. C. Prince, R. Richter, M. Vondracek, R. Camilloni, L. Avaldi, M. Coreno, G. Stefani, C. Furlani, M. de Simone, S. Stranges and M.-Y. Adam, *Journal of Electron Spectroscopy and Related Phenomena*, 1999, **101**, 959.

32 H. J. Svec and D. D. Clyde, *Journal of Chemical and Engineering Data*, 1965, **10**, 151.

33 C. G. de Kruif, J. Voogd and J. C. A. Offringa, *The Journal of Chemical Thermodynamics*, 1979, **11**, 651.

34 F. Filsinger, G. Meijer, H. Stapelfeldt, H. N. Chapman and J. Küpper, *Physical Chemistry Chemical Physics*, 2011, **13**, 2076.

35 O. Kornilov, M. Eckstein, M. Rosenblatt, C. P. Schulz, K. Motomura, A. Rouzée, J. Klei, L. Foucar, M. Siano, A. Lübcke, F. Schapper, P. Johnsson, D. M. P. Holland, T. Schlatholter, T. Marchenko, S. Düsterer, K. Ueda, M. J. J. Vrakking and L. J. Frasinski, *Journal of Physics B*, 2013, **46**, 164028.

36 L. J. Frasinski, V. Zhaunerchyk, M. Mucke, R. J. Squibb, M. Siano, J. H. D. Eland, P. Linusson, P. van der Meulen, P. Salén, R. D. Thomas, M. Larsson, L. Foucar, J. Ullrich, K. Motomura, S. Mondal, K. Ueda, T. Osipov, L. Fang, B. F. Murphy, N. Berrah, C. Bostedt, J. D. Bozek, S. Schorb, M. Messerschmidt, J. M. Glownia, J. P. Cryan, R. Coffee, O. Takahashi, S. Wada, M. N. Piancastelli, R. Richter, K. C. Prince and R. Feifel, *Physical Review Letters*, 2013, **111**, 073002.

37 N. Rohringer and R. Santra, *Physical Review A*, 2008, **77**, 053404.
38 P. Meystre and M. Sargent III, *Elements of Quantum Optics*, Springer, 1991.
39 A. I. Kuleff and L. S. Cederbaum, *Chemical Physics*, 2007, **338**, 320.